

PROBING CONVECTION AND SOLAR ACTIVITY WITH LOCAL HELIOSEISMOLOGY

L. Gizon

Max-Planck-Institut für Sonnensystemforschung, 37191 Katlenburg-Lindau, Germany

ABSTRACT

Methods of local helioseismology provide three-dimensional images of the solar interior, giving insight about the subsurface structure and dynamics of convective structures and magnetic regions. Local helioseismology largely owes its success and fast development to the MDI data that have been collected by SOHO over the last ten years. Here I discuss in some detail what we have learned about the evolution and the lifetime of the supergranulation pattern, the variation of the wave speed under active regions and sunspots, and the connections between flows and magnetic activity. Interpreting seismic measurements is a challenging aspect of local helioseismology. Future progress will come from improved models of the sensitivity of the observations to localized perturbations in the Sun, including the effect of strong magnetic fields.

Key words: Helioseismology.

1. INTRODUCTION

Local helioseismology is a set of techniques to probe the three-dimensional structure and the evolution of the near surface layers of the Sun (see e.g. Gizon & Birch, 2005, for a recent review). Local methods rely on precise measurements of wave travel times, mode frequency shifts, and scattering phase shifts, to name a few. At the time of SOHO's launch, many of these methods had already been proposed to study the interaction of solar waves with localized structures in solar interior, in particular large-scale convective structures and magnetised regions (e.g. Hill, 1988; Braun & Duvall, 1990; Lindsey & Braun, 1990; Duvall et al., 1993). In fact, the first 3D tomographic inversions had just appeared (Kosovichev, 1996). Yet, it is no exaggeration to say that SOHO observations, which are free of atmospheric noise, nearly continuous and high-resolution, have revolutionized the field of local helioseismology. An early example is the demonstration by Duvall et al. (1997) that information about subsurface inhomogeneities can be retrieved at supergranular scales.

The intent of this paper is not to provide a complete review of the field, but instead to present a personal selec-

tion of interesting inferences made possible by the MDI-SOHO observations (Scherrer et al., 1995). Section 2 discusses convection and, in particular, time-distance measurements of supergranular flows: structure, lifetimes, and coupling to rotation. The seismology of sunspots and active regions is discussed in Section 3. Comments are included here and there to remind us that the limitations faced today by local helioseismology have little to do with lack of quality data but are largely due to an oversimplified interpretation of the seismic measurements.

2. CONVECTION

2.1. Divergence maps

The simplest way to detect near-surface convective structures is to measure, with a cross-correlation technique, the time it takes for solar waves to propagate between any given point on the solar surface and a concentric annulus around that point. The difference in travel times between inward and outward propagating waves is a measure of the local divergence of the flow (Duvall et al., 1997). In the case of surface-gravity waves (f modes), the travel-time difference is directly sensitive to the horizontal divergence of the flow velocity in the top 2 Mm below the surface (Duvall & Gizon, 2000). The holographic technique (Braun & Lindsey, 2003) also provides divergence maps that look very similar.

Figure 1a shows the divergence signal (inward minus outward travel times) obtained by analyzing a 12-hr long time series of MDI full-disk Doppler velocity images tracked at the Carrington rate to remove the main component of solar rotation. The mean radius of the annulus is $\Delta = 15$ Mm. A white, or positive signal, corresponds to a horizontal outflow. From the size of the features present, supergranulation is identified as the main contributor to the signal. Compared to the Doppler line-of-sight velocity, the main advantage of the time-distance divergence signal is that it is essentially free of systematic variations across the field of view, which is a very important condition to study the evolution of the pattern.

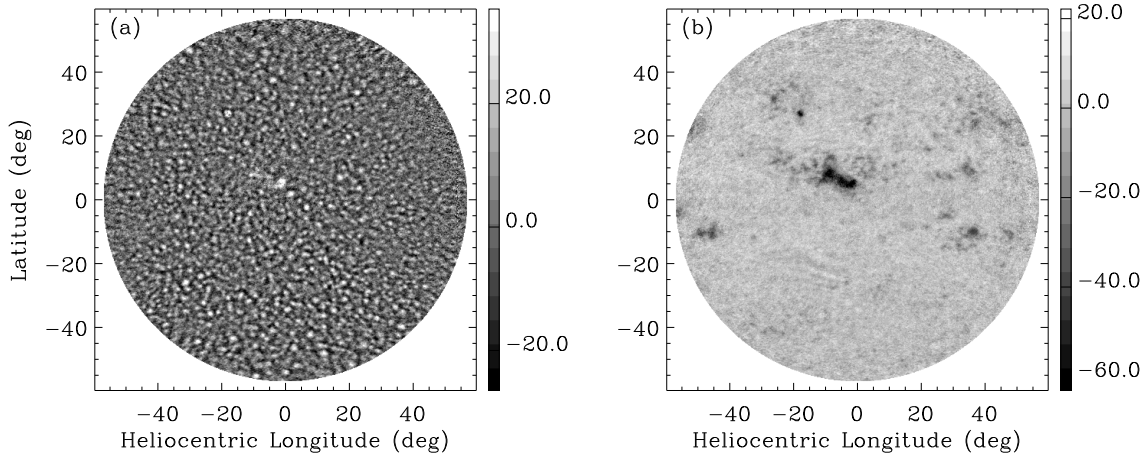


Figure 1. (a) Map of the horizontal divergence of the flows in a 1-Mm deep layer below the photosphere. Center-to-annulus f-mode travel-time differences are measured in units of second (observation duration $T = 12$ hr, annulus radius $\Delta = 15$ Mm, MDI full-disk data). A positive signal corresponds to a positive divergence (b) Mean travel times (average between inward and outward propagating waves) measured with respect to the quiet Sun value. Travel times are reduced in regions of magnetic activity.

2.2. Spatial power

The fact that supergranulation dominates the divergence signal is readily seen in the spatial power spectrum of the data, which shows a pronounced peak near wavenumbers $k \sim 120/R_{\odot}$. In addition, spatial power is seen at much lower and much higher wavenumbers. To assess the physical reality of the signal at both ends of the spectrum, it is important to have a quantitative estimate of the background noise due to the stochastic nature of the solar oscillations. Such a model was derived by Gizon & Birch (2004) from first principles.

Figure 2 shows the observed power for a center-to-annulus f-mode divergence map derived from a short time series ($T = 2$ hr) of MDI high-resolution Dopplergrams. The noise model indicates that most of the power at $k > 300/R_{\odot}$ is not due to wave scattering by small-scale convection. Specific averaging procedures must be employed to study, for example, the effect of large granules on oscillations (Duvall, private communication). Alternatively, the data can be inverted using appropriate wave-based sensitivity kernels (e.g. Birch, 2004, and §2.5). It can be shown, however, that there is an absolute limit to how small a feature can be detected: travel times contain no information on convective wavelengths smaller than $\lambda_w/2$, where λ_w is the dominant wavelength of the solar oscillations used to probe the Sun (Gizon & Birch, 2004). Taking a 3-mHz f mode as a reference, this condition is equivalent to

$$k < \frac{4\pi}{\lambda_w} = \frac{1800}{R_{\odot}} \left(\frac{5 \text{ Mm}}{\lambda_w} \right). \quad (1)$$

As for the low spatial wavenumbers, it seems quite safe to say that power is detectable down to $k \sim 40/R_{\odot}$. For even smaller values of k , one must worry about large-scale systematic errors introduced by the optical distor-

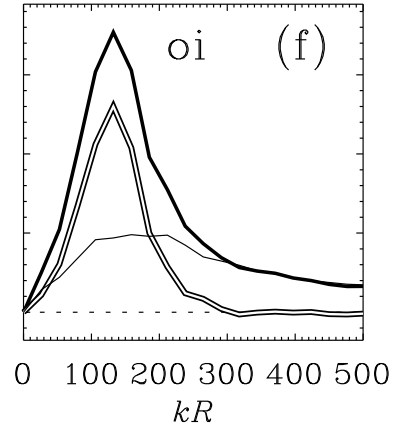


Figure 2. Spatial power spectrum of the divergence signal (f modes, observation duration $T = 2$ hr, annulus radius $\Delta = 5$ Mm) versus wavenumber k in units of $1/R_{\odot}$. The thick line shows the MDI observations and the thin line shows the noise background computed from the model of Gizon & Birch (2004). The difference between the observations and the noise background is given by the double line. The power is plotted on a linear scale.

sions of the telescope. Both time-distance helioseismology and ring diagram analysis have revealed the existence of long-lived, large scale flow patterns that may be related to the largest scales of deep convection (Gizon et al., 2001; Haber et al., 2001; Toomre, 2002).

2.3. Evolution and lifetimes

The evolution of the pattern of convection has been studied using long sequences (two to three months each year) of divergence maps as shown in Figure 1a. Each map

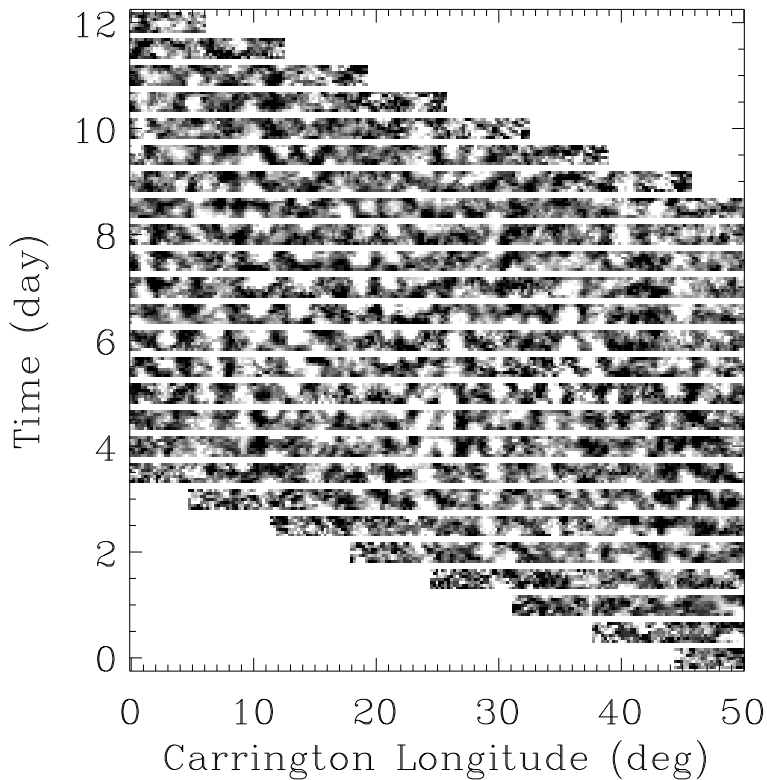


Figure 3. Evolution of the divergence signal (as defined in Figure 1a) with a time step of 12 hr. Each strip corresponds to a longitudinal section of the data centered at latitude 15° and 1.68° wide. Supergranules (white regions of positive divergence) can be traced over several days.

is an average over 12 hr and covers a region of size $120^\circ \times 120^\circ$ centered on the solar disk. This means that a feature co-rotating with the Sun can be observed continuously for about 9 days. Such a long time series enabled Gizon et al. (2003) and Gizon & Duvall (2003) to resolve unexpected oscillations in the 3D the spectrum of the divergence signal (with frequencies ν_0 in the range 1-2 μHz) and excess power in the prograde direction. These wave-like properties, which have recently been confirmed by D. C. Braun using divergence maps obtained with acoustic holography, have not been explained so far. An interesting analysis by Green & Kosovichev (2006) suggests that convection in a shear flow could take the form of travelling waves.

These time-distance data are also ideal to study the lifetime of supergranulation. The evolution of the pattern is shown in Figure 3. We find that the lifetime of features with $k = 120/R_\odot$ is about 2 days: the lifetime of supergranulation would appear to have been underestimated in the past. The reason for this has to do with the observed oscillation of the autocorrelation function (Beck & Duvall, 2001) with a period of about 6 days ($1/\nu_0$). The lifetime of 2 days corresponds to the e -folding lifetime of the *envelope* of the autocorrelation function, while earlier estimates were based on the assumption that the autocorrelation function exhibits a simple exponential decay in time (Harvey, 1985).

2.4. Coupling to rotation

In addition to the horizontal divergence, 'div', it is also possible to measure separately the two horizontal components of the vector flow (by splitting the annulus into quadrants), from which an estimate of the vertical vorticity, 'curl', can be derived. After removing the large-scale vorticity due to differential rotation and meridional circulation, Gizon et al. (2003) found a small correlation between div and curl of the form

$$\langle \text{div curl} \rangle \simeq -3 \times 10^{-10} \sin(\lambda) \Omega(\lambda) / \Omega_{\text{eq}} \text{ s}^{-2}, \quad (2)$$

where $\Omega(\lambda)$ is the angular velocity of the Sun at latitude λ , and Ω_{eq} is the equatorial angular velocity. The latitudinal variation of the correlation is precisely what is expected of the effect of the Coriolis force on convection (see Rüdiger et al., 1999, for a quasi-linear theory). In the northern hemisphere, supergranular cells rotate preferentially clockwise where the horizontal divergence is positive, while they rotate preferentially counterclockwise in the convergent flows near the sinks. The sense of circulation is reversed in the southern hemisphere. The convection-rotation coupling is weak (the correlation coefficient between div and curl is less than 2%), in agreement with numerical simulations (Hathaway, 1982; Egorov et al., 2004). We note that the measurements (Eq. [2]) should provide an independent constraint on the lifetime of supergranulation.

2.5. Finite-wavelength tomography

In order to gain access to spatial scales that are smaller than supergranulation, it is necessary to consider sophisticated inversion schemes. Two issues have to be addressed: (i) the variation in time of the flows over the integration time, T , of the observations and (ii) the spatial variations of the flows over scales that are smaller than the dominant wavelength of solar oscillations. For the sake of simplicity, I will assume that the lifetime of the convective structures that we want to study is larger than T , i.e. ignore (i), and explain in simple terms why issue (ii) matters.

Seismic observations and steady perturbations in solar internal properties are connected through finite-wavelength sensitivity kernels. The central lobe of a sensitivity kernel is called the first Fresnel zone: a scatterer placed on the boundary of the first Fresnel zone causes a phase difference between the direct and scattered waves of π . To a first approximation, one may assume that this phase difference arises only from a change in the geometrical path length, δx . An estimate of the width of the Fresnel zone, L_F , thus follows from the condition $\delta x \sim \lambda_w/2$, where λ_w is the dominant wavelength of the solar oscillations under consideration. For the simple case of a uniform medium and in the limit $\Delta \gg \lambda_w$, the change in path length due to a scatterer at equal distance between the source and the receiver is $\delta x = (\Delta^2 + L_F^2)^{1/2} - \Delta \simeq L_F^2/(2\Delta)$, which gives

$$L_F \sim (\lambda_w \Delta)^{1/2}. \quad (3)$$

To illustrate this point, we may take as a reference for λ_w the wavelength of an f mode near 3 mHz:

$$L_F \sim 10 \text{ Mm} \left(\frac{\lambda_w}{5 \text{ Mm}} \right)^{1/2} \left(\frac{\Delta}{20 \text{ Mm}} \right)^{1/2}. \quad (4)$$

Thus, the width of the first Fresnel zone does exceed the size of some of the solar convective structures that leave a signature in the travel-time measurements. To be more precise, finite-wavelength effects become very important when

$$k > \frac{\pi}{L_F}, \quad (5)$$

where k is a convective wavenumber. This condition is equivalent to

$$kR_\odot > 220 \left(\frac{5 \text{ Mm}}{\lambda_w} \right)^{1/2} \left(\frac{20 \text{ Mm}}{\Delta} \right)^{1/2}, \quad (6)$$

which shows that it is required to have a finite-wavelength theory if we are to correctly interpret travel-time anomalies caused by small supergranules.

Finite-wavelength tomography has received a lot attention in geophysics in the last few years. The extension to solar physics is well under way (Jensen et al., 2000; Birch & Kosovichev, 2000; Gizon & Birch, 2002; Birch, 2004; Birch et al., 2004; Braun et al., 2004). One of the differences between helio- and geo-seismology is that in the

Sun waves are excited stochastically over the whole solar surface. Furthermore, there are important differences in the way seismic measurements are recorded. For instance, solar data are affected by foreshortening and line-of-sight projection effects leading to a systematic center-to-limb dependence in the sensitivity kernels (Jackiewicz et al., 2006).

3. MAGNETIC ACTIVITY

3.1. Perturbations

Observations have shown that the frequencies, phases, and amplitudes of solar oscillations are perturbed in regions of enhanced magnetic activity.

Figure 1b shows a map of f-mode travel-time perturbations associated with a large active region. The mean travel times, averaged for waves travelling both outward from the center of the annulus and inward, are decreased in the active region. This is usually interpreted as evidence for an increase in wave speed.

Figure 4 shows results obtained with acoustic imaging, a technique used to reconstruct the seismic signal at any target point on the solar surface (or in the solar interior) from the signal measured everywhere on the solar surface. The reconstructed signal contains information about the amplitude and phase of wavepackets converging toward the target point or diverging from that point. Active regions introduce local changes easily seen in maps of the reconstructed outgoing intensity and phase shifts. Waves are absorbed by active regions as evidenced by the deficit of outgoing acoustic intensity. In Figure 4 the largest phase-time shift is 1.5 min, i.e. a significant fraction of the wave oscillation periods. Similar results are obtained with acoustic holography.

3.2. Structure of active regions

The forward and inverse problems of sunspot seismology are not trivial. A number of simplifications have been used to obtain approximate answers. The first assumption which is commonly used is that sunspot perturbations are small. In addition, it is often assumed that the travel-time shifts, scattering phase shifts, or local mode frequency shifts are caused by sound speed perturbations (indirect effect of the magnetic field). Under these simplifying assumptions, a linear inverse problem can be solved to infer subsurface sound-speed perturbations (e.g. Kosovichev et al., 2000). One of the latest inversions (Kosovichev, 2004), using high-resolution MDI-SOHO data, is shown in Figure 5. It is found that the sound speed is lower just below the sunspot (probably indicating a lower temperature), while the sound speed is higher at depths greater than about 4 Mm. These findings indicate that a sunspot is a rather shallow phenomenon. The vertical

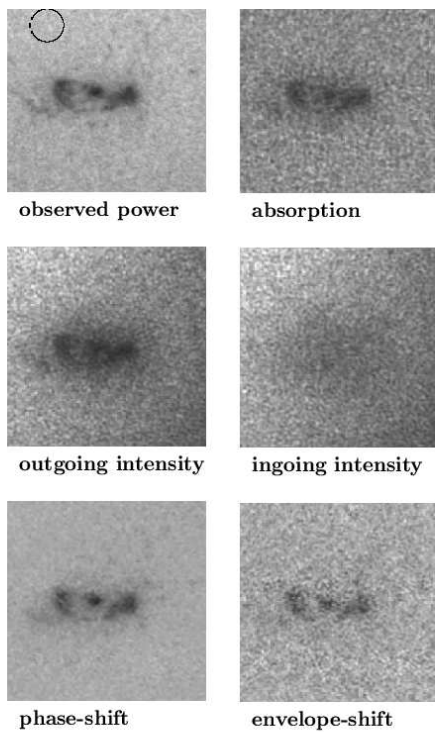
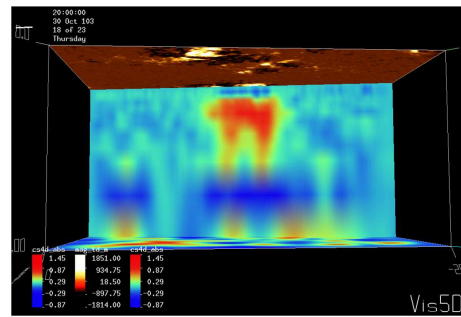


Figure 4. Reduction in acoustic power, enhanced absorption, deficit of outgoing intensity, unaffected ingoing intensity, decrease in phase and envelope shifts in active region NOAA 7978, as measured with acoustic imaging (Chou, 2000). An MDI time series of duration 2000 min was used. The data were filtered with a Gaussian filter of FWHM= 1 mHz centered at 3.5 mHz. The acoustic power is reduced by a factor of 4 in the central sunspot. The size of the aperture used is $2\text{-}6^\circ$ (a two-degree circle is shown in the upper left map). The dimension of each map is 24.0° in longitude and 24.7° in latitude.

cut through the pair of sunspots with opposite polarities (Fig. 5) reveals a very interesting loop-like structure.

Some of the assumptions used in current inversions are not quite reasonable. A first improvement is expected from using wave-based sensitivity kernels, as opposed to ray kernels (e.g. Couvidat et al., 2004). Numerical models indicate that acoustic waves passing through sunspots suffer strong perturbations and partial conversion to magneto-acoustic waves (e.g. Cally & Bogdan, 2003; Cally, 2005): surface perturbations are not small. Also, sound-speed perturbations are not the only perturbations which enter the problem. For example, density changes (Wilson depression) and the direct effect of the magnetic field through the Lorentz force. Basu et al. (2004) performed a depth inversion of local frequency shifts for the sound speed and the first adiabatic exponent, simultaneously (see Figure 6). According to Basu et al. (2004), at least part of the differences between active and quiet regions is likely to be due to the structural and thermal perturbations caused by magnetic fields.



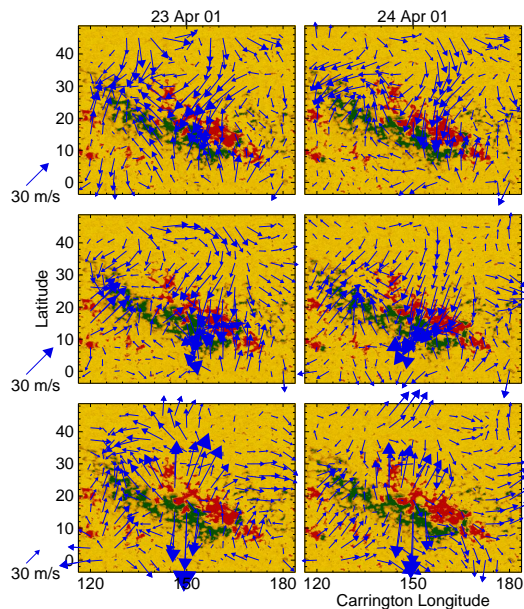


Figure 7. Ring-diagram OLA inversion of horizontal flows below an active region on April 23 (left panels) and April 24 (right panels). The depths shown are 1 Mm (top panels), 7 Mm (middle panels), and 14 Mm (bottom panels). Note the presence of a collimated jet oriented north-south. From Haber et al. (2004).

On a much larger scale, long time averages of surface flow maps reveal 50 m/s horizontal flows that converge toward active regions (Gizon et al., 2001; Haber et al., 2001). These flows extend as far as 30° away from the centers of active regions. On the other hand, deeper inside the Sun (10 Mm or more), inversions point to the existence of horizontal flows diverging from active regions (Haber et al., 2004; Zhao & Kosovichev, 2004). This is illustrated in Figure 7. A model by Spruit (2003) predicts a surface inflow toward magnetic regions driven by a decrease in gas pressure there. These flows introduce a solar-cycle variation in the mean meridional circulation, which may affect the large-scale transport of the surface magnetic flux (Gizon, 2004). Using a mass conservation constraint, Komm et al. (2004) derived the vertical component of velocity and the kinetic helicity density, which are also connected to surface magnetic activity.

3.4. Flares and sunquakes

Kosovichev & Zharkova (1998) detected a sunquake triggered by an X-class flare. The evolution of the circular wavefront followed the time-distance curve for acoustic waves. Donea et al. (1999) showed that the same sunquake was most easily detectable at frequencies around 6 mHz. As discussed by Zharkova (2006), several other sunquakes have been discovered since: they contain a wealth of information about the physics of energy release by solar flares.

3.5. Far-side imaging

Far-side imaging is a special case of phase-sensitive holography. The idea is to use the observations collected on the visible hemisphere of the Sun to learn about the presence of active regions on the far side of the Sun (Lindsey & Braun, 2000). It uses waves that leave the front side, bounce once then bounce from a target location (on the far side) then bounce again on the way returning to the front side where we can see them again. This 2+2 skip geometry is designed to map regions near the antipode of the center of the visible disk. For focus positions closer to the limb, Braun & Lindsey (2001) proposed to use a 1+3 skip geometry. By combining the 2+2 and 1+3 skip geometries, Oslund & Scherrer (2001) showed that we can map the entire farside – a remarkable achievement. Active regions on the far side introduce travel-time deficits of the order of ten seconds with respect to the quiet Sun. Far-side imaging provides reliable information about large active regions, and is thus important for space weather predictions.

3.6. In search of the seismic signature of the magnetic field

A major goal of helioseismology is to detect and image the magnetic field in the solar interior. This has not been accomplished yet. In this section, I list a few ideas that may deserve to be explored.

It is accepted that a knowledge of the frequencies of the global modes of oscillations is not sufficient to disentangle magnetic perturbations from other aspherical perturbations (Zweibel & Gough, 1995); global-mode frequencies can only provide upper limits on the strength of a buried magnetic field (e.g. Basu, 1997). The specific signature of the magnetic field resides in the anisotropic distortion to the eigenfunctions. For this reason, it is useful to turn to methods of local helioseismology. In time-distance helioseismology, an estimate of the local wave speed is obtained by considering a travel-time average over all ray paths that intersect at a target location. To first order, magnetic fields affect mean travel-time perturbations, not travel-time differences. The difficulty is to separate unambiguously magnetic perturbations from other perturbations that also affect wave travel times, such as temperature and density inhomogeneities but also spatial variations in the wave excitation and damping.

3.6.1. Anisotropic wave propagation

In order to provide a simple illustration of the specificity of the dependence of travel-time measurements on magnetic perturbations, we consider the effect of a uniform horizontal magnetic field, $\mathbf{B} = (B_x, B_y)$, on the propagation of surface gravity waves at the interface of a half-space with uncompressed density, ρ . According to Chan-

drasekhar (1961), the dispersion relation is

$$(\omega - \mathbf{k} \cdot \mathbf{u})^2 = gk + 2(\mathbf{k} \cdot \mathbf{a})^2, \quad (7)$$

where the Alfvén velocity vector is defined by

$$\mathbf{a} = \mathbf{B} / \sqrt{4\pi\rho}. \quad (8)$$

Also included in equation (7) is the Doppler shift due to a uniform horizontal flow, \mathbf{u} . The magnetic field introduces an effective surface tension, which depends on the angle between \mathbf{B} and the horizontal wavevector \mathbf{k} . We note that the coefficient in front of the term $(\mathbf{k} \cdot \mathbf{a})^2$ in equation (7) is model dependent (e.g. Bijlsma, 1970; Miles & Roberts, 1992).

Let us denote by $\omega_0 = \sqrt{gk}$ the unperturbed wave frequency at resonance. Under the assumption that the magnetic field is weak ($a \ll \omega_0/k$), we may linearize the dispersion relation to obtain the frequency change due to both \mathbf{B} and \mathbf{u} :

$$\delta\omega(\mathbf{k}) \simeq \mathbf{k} \cdot \mathbf{u} + \frac{(ka)^2}{2\omega_0} \left[1 + \cos(2\hat{\mathbf{k}} \cdot \hat{\mathbf{a}}) \right]. \quad (9)$$

The magnetic field introduces an isotropic frequency shift and a frequency perturbation which varies like the cosine of twice the angle between \mathbf{k} and \mathbf{B} , while the flow introduces a Doppler shift which varies like the cosine of the angle between \mathbf{k} and \mathbf{u} . In the spirit of Ryutova & Scherrer (1998), we project the azimuthal dependence of the frequency shifts onto an orthogonal basis of circular functions to separate the various azimuthal components:

$$\delta\omega_m(k) = \frac{1}{2\pi} \int_0^{2\pi} \delta\omega(\mathbf{k}) e^{im\theta} d\theta, \quad m = 0, 1, \dots, \quad (10)$$

where the integration variable θ is the angle between \mathbf{k} and the horizontal direction $\hat{\mathbf{x}}$. For our simple problem, this decomposition is convenient as it leads to the trivial inversion

$$u_x + iu_y = 2\delta\omega_1/k, \quad (11)$$

$$a_x + ia_y \simeq \pm 2(\omega_0\delta\omega_2)^{1/2}/k. \quad (12)$$

This is illustrated in Figure 8: the vector flow, \mathbf{u} , is fully specified by the coefficient $\delta\omega_1$, while the coefficient $\delta\omega_2$ specifies the direction, $(\arg \delta\omega_2)/2$, and the magnitude of \mathbf{B} , but not its sense.

The magnetic field also affects the isotropic average $\delta\omega_0$, but so do other types of perturbations like temperature and density. Current local helioseismology techniques, based on the $m = 0$ and $m = 1$ averages only, are unable to disentangle these various perturbations. At first sight, it would seem easy to generalized travel-time measurements to include terms with $m > 1$. A possible application would be to map the local wave speed in a sunspot's penumbra, where the magnetic field is mostly horizontal. One finds that, indeed, there is a difference in travel time for waves propagating across and along magnetic field lines. Unfortunately, this apparent wave

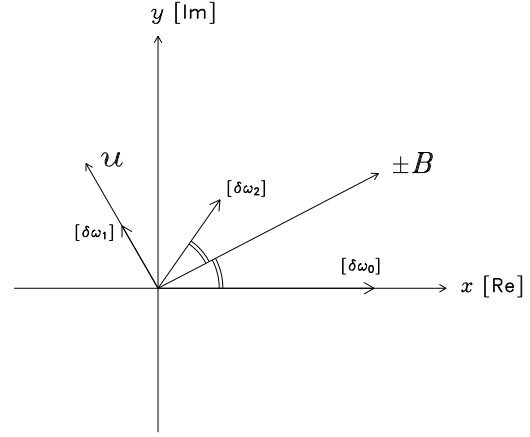


Figure 8. Graphical representation of the complex coefficients, $\delta\omega_m$, of the multipole expansion of the azimuthal dependence of f-mode frequency shifts.

speed anisotropy is dominated by a completely unrelated effect: inhomogeneous wave damping. The higher frequency waves that travel through the sunspot are damped by the sunspot. This implies that the frequency content of wavepackets in the vicinity of sunspots depends on their direction of propagation. This effect, in combination with wave dispersion and the presence of the moat flow, makes it difficult to unambiguously extract the wave-speed anisotropy introduced by the penumbral magnetic field. Another possibility would be to search for the signature of a large scale toroidal magnetic field deeper in the convection zone. In particular, one could extend the work of Chou & Serebryanskiy (2002) without averaging over the direction of wave propagation. Here again, travel-time anisotropies may be polluted by a surface contribution from active regions, which are not homogeneously distributed over the solar surface.

3.6.2. Scattering by small magnetic features

A promising approach, pioneered by Duvall et al. (2006a), is to study the small magnetic features which form the magnetic network, as seen in MDI high resolution magnetograms averaged over 4 hr intervals. Network elements have the advantage of being relatively simple magnetic configurations. In addition, they are so many that a statistical treatment is possible. Duvall et al. (2006a) found the decrease in f-mode travel time caused by an average magnetic feature to be 2 s Mm^{-2} at most. It is hoped that the observed travel time maps will help us understand wave scattering by slender vertical flux tubes, by comparison with models (Bogdan et al., 1996). The first Born approximation may prove useful to obtain approximate answers (Gizon et al., 2006b). For a discussion of the study of small magnetic features by means of local helioseismology, see Duvall et al. (2006b).

4. CONCLUSION

Local helioseismology with MDI-SOHO has revealed unexpected aspects of the dynamics of supergranulation as well as wave-speed anomalies and complex flow patterns below sunspots and active regions. Future progress is likely to come from improved models of the interaction of seismic waves with subsurface inhomogeneities and validation through realistic numerical simulations (e.g. Werne et al., 2004).

REFERENCES

- Basu S., 1997, *MNRAS* 288, 572
- Basu S., Antia H. M., Bogart R. S., 2004, *ApJ* 610, 1157
- Beck J. G., Duvall T. L., 2001, *ESA SP-464*, 577
- Biljlsma S. J., 1970, *Plasma Phys.* 13, 681
- Birch A. C., 2004, *ESA-SP 559*, 138
- Birch A. C., Kosovichev A. G., 2000, *Solar Phys.* 192, 193
- Birch A. C., Kosovichev A. G., Duvall T. L., 2004, *ApJ* 608, 580
- Bogdan T. J., Hindman B. W., Cally P. S., 1996, *ApJ* 465, 406
- Braun D. C., Birch A. C., Lindsey C., 2004, *ESA SP-559*, 337
- Braun D. C., Duvall T. L., 1990, *Solar Phys.* 129, 83
- Braun D. C., Lindsey C., 2001, *ApJ* 560, L189
- Braun D. C., Lindsey C., 2003, *ESA SP-517*, 15
- Cally P. S., 2005, *MNRAS* 358, 353
- Cally P. S., Bogdan T. J., 2003, *ApJ* 402, 721
- Chandrasekhar, S., *Hydrodynamic and hydromagnetic stability* (Oxford: Clarendon), 464
- Chou D.-Y., 2000, *Solar Phys.* 192, 241
- Chou D.-Y., Serebryanski A., 2002, *ApJ* 578, L157
- Couvidat S., Birch A. C., Kosovichev A. G., Zhao J., 2004, *ApJ* 607, 554
- Donea A.-C., Braun D. C., Lindsey C., 1999, *ApJ* 513, L143
- Duvall T. L., Birch A. C., Gizon L., 2006a, *ApJ*, in press
- Duvall T. L., D'Silva S., Jefferies S. M., Harvey J. W., Schou J., 1996, *Nature* 379, 235
- Duvall T. L., Gizon L., 2000, *Solar Phys.* 192, 177
- Duvall T. L., Jefferies S. M., Harvey J. W., Pomerantz M. A., 1993, *Nature* 362, 430
- Duvall T. L., Kosovichev A. G., Scherrer P. H. et al., 1997, *Solar Phys.* 170, 63
- Duvall T. L. et al., 2006b, this volume
- Egorov P., Rüdiger G., Ziegler U., 2004, *A&A* 425, 725
- Gizon L., 2004, *Solar Phys.* 224, 217
- Gizon L., Birch A. C., 2002, *ApJ* 571, 966
- Gizon L., Birch A. C., 2004, *ApJ* 614, 472
- Gizon L., Birch A. C., 2005, *Living Rev. Solar Phys.* 6, 2
- Gizon L., Duvall T. L., 2003, *ESA-SP 517*, 43
- Gizon L., Duvall T. L., 2004, *IAU Symp.* 223, 41
- Gizon L., Duvall T. D., Larsen R. M., 2000, *J. Astrophys. Astron.* 21, 339
- Gizon L., Duvall T. D., Larsen R. M., 2001, *IAU Symp.* 203, 189
- Gizon L., Duvall T. D., Schou J., 2003, *Nature* 421, pp. 43-44 and 764.
- Gizon L., Hanasoge S. M., Birch A. C., 2006b, *ApJ* 643, 549
- Gizon L., Jackiewicz J., Birch A. C., Duvall T. L., 2006a, in *Solar activity: exploration, understanding and prediction* (Lund, Sweden), *ESA CD*
- Green C. A., Kosovichev A. G., 2006, *ApJ* 641, L77
- Haber D. A., Hindman B. W., Toomre J., Bogart R. S., Hill F., 2001, *ESA SP-464*, 209
- Haber D. A., Hindman B. W., Toomre J., Thompson M. J., 2004, *Solar Phys.* 220, 371
- Hathaway D. H., 1982, *Solar Phys.* 77, 341
- Harvey J., 1985, *ESA SP-235*, 199
- Hill F., 1988, *ApJ* 333, 996
- Jackiewicz J., Gizon L., Birch A. C., 2006, this volume
- Jensen J. M., Jacobsen B. H., Christensen-Dalsgaard J., 2000, *Solar Phys.* 192, 231
- Komm R., Corbard T., Durney B. R., González Hernández I., Hill F., Howe R., Toner C., 2004, *ApJ* 605, 554
- Kosovichev A. G., 1996, *ApJ* 461, L55
- Kosovichev A. G., 2004, *IAU Symp.* 223, 171
- Kosovichev A. G., Duvall T. L., Scherrer P. H., *Solar Phys.* 192, 159
- Kosovichev A. G., Zharkova V. V., 1998, *Nature* 393, 317
- Lindsey C., Braun D. C., 1990, *Solar Phys.* 126, 101
- Lindsey C., Braun D. C., 2000, *Science* 287, 1799
- Lindsey C., Braun D. C., Jefferies S. M., Woodard M. F., Fan Y., Gu Y., Redfield S., 1996, *ApJ* 470, 636
- Miles A. J., Roberts B., 1992, *Solar Phys.* 141, 205
- Rüdiger G., Brandenburg A., Pipin V. V., 1999, *Astron. Nachr.* 320, 135
- Ryutova M., Scherrer P. H., 1998, *ApJ* 494, 438
- Scherrer P. H., Bogart R. S., Bush R. I. et al., 1995, *Solar Phys.* 162, 129
- Spruit H. C., 2003, *Solar Phys.*, 213, 1
- Toomre J., 2002, *Science* 296, 64
- Werne J., Birch A. C., Julien K., 2004, *ESA-SP 559*, 172
- Zweibel E. G., Gough D. O., 1995, in *ESA SP-372*, Vol. 2, 73
- Zhao J., Kosovichev A. G., 2004, *ApJ* 607, L135
- Zhao J., Kosovichev A. G., Duvall T. L., 2001, *ApJ* 557, 384
- Zharkova V. V., 2006, this volume